

Article

Mid-IR Intraband Photodetectors with Colloidal Quantum Dots

Xue Zhao ¹ , Ge Mu ¹, Xin Tang ^{1,2,3} and Menglu Chen ^{1,2,3,*}

¹ School of Optics and Photonics, Beijing Institute of Technology, Beijing 100081, China; 3220210544@bit.edu.cn (X.Z.); 7520210145@bit.edu.cn (G.M.); xintang@bit.edu.cn (X.T.)

² Beijing Key Laboratory for Precision Optoelectronic Measurement Instrument and Technology, Beijing 100081, China

³ Yangtze Delta Region Academy of Beijing Institute of Technology, Jiaxing 314019, China

* Correspondence: menglu@bit.edu.cn

Abstract: In this paper, we investigate an intraband mid-infrared photodetector based on HgSe colloidal quantum dots (CQDs). We study the size, absorption spectra, and carrier mobility of HgSe CQDs films. By regulating the time and temperature of the reaction during synthesis, we have achieved the regulation of CQDs size, and the number of electrons doped in conduction band. It is experimentally verified by the field effect transistor measurement that dark current is effectively reduced by a factor of 10 when the 1Se state is doped with two electrons compared with other doping densities. The HgSe CQDs film mobility is also measured as a function of temperature the HgSe CQDs thin film detector, which could be well fitted by Marcus Theory with a maximum of $0.046 \pm 0.002 \text{ cm}^2/\text{Vs}$ at room temperature. Finally, we experimentally discuss the device performance such as photocurrent and responsivity. The responsivity reaches a maximum of $0.135 \pm 0.012 \text{ A/W}$ at liquid nitrogen temperature with a narrow band photocurrent spectrum.

Keywords: intraband photodetector; colloidal quantum dot; HgSe; mid-infrared



Citation: Zhao, X.; Mu, G.; Tang, X.; Chen, M. Mid-IR Intraband Photodetectors with Colloidal Quantum Dots. *Coatings* **2022**, *12*, 467. <https://doi.org/10.3390/coatings12040467>

Academic Editor: Ana-Maria Lepadatu

Received: 28 February 2022

Accepted: 23 March 2022

Published: 30 March 2022

Publisher's Note: MDPI stays neutral with regard to jurisdictional claims in published maps and institutional affiliations.



Copyright: © 2022 by the authors. Licensee MDPI, Basel, Switzerland. This article is an open access article distributed under the terms and conditions of the Creative Commons Attribution (CC BY) license (<https://creativecommons.org/licenses/by/4.0/>).

1. Introduction

In recent years, colloidal quantum dots (CQDs) devices have gradually been widely used in imaging, remote sensing, gas detection, medical diagnosis, and epidemic prevention and control [1–4]. The performance of CQDs photodetectors has been comparable to commercial InGaAs photodiodes but order-of-magnitude reduction in cost [5]. Compared traditional infrared photodetectors, CQDs photodetectors theoretically offer the advantages of higher operating ambient temperatures, smaller dark currents, faster response performance [6], and lower fabrication cost [7].

The materials selected for the infrared photodetectors with interband transition [8,9] are usually limited in semimetal or ternary alloy with a small gap [10]. However, the intraband CQD devices, utilizing optical transitions from lowest electron state labelled 1Se and the next level 1Pe, hold unique promise to extend the wavelength from near- and mid-infrared to long-wave infrared (Supplementary Materials Figure S1). What is more, intraband photodetectors promise a better photoelectric performance [11,12] due to the low conduction band density which inhibit the process of Auger relaxation [13–16]. For example, the Auger relaxation coefficient is at least three orders smaller in intraband HgSe CQDs compared with the bulk materials with the same energy gap [17]. Hence, the study of CQDs intraband photodetectors has important research significance. The air stable n-type mercury (ii) selenide (HgSe) CQDs provide an excellent platform for studying intraband photodetectors [18,19].

In current stage, due to the limited study on intraband materials, the intraband photodetectors based in HgSe CQDs have excessive dark current compared to interband CQD photodetectors at the same wavelength. The solution is to precisely adjust the number of electrons in 1Se [11,20]. The unpaired electrons in Se state or Pe state would result

in large dark current. The dark current is minimal when 1Se is fully filled which is two electrons in conduction band per CQD (Supplementary Materials).

To address these challenges, in this paper, we provide a way to control the doping inside the HgSe CQDs, which is characterized by optical and transport measurements. Then, we build the HgSe CQDs intraband photodetector in mid-infrared (Mid-IR) and further analyze its photocurrent, and responsivity.

2. Materials and Methods

In a glove box with a nitrogen environment, 27.2 mg of mercury chloride (HgCl_2) and 4 mL of oleylamine (OAm) were placed in a 40 mL vial, and were heated at $100\text{ }^\circ\text{C}$ for 1 h, and then were heat-balanced at $115\text{ }^\circ\text{C}$ (or $120\text{ }^\circ\text{C}$) for half an hour. A total of 126 mg (0.1 mmol) of selenium urea was dissolved in 10 mL of OAm and heated at $180\text{ }^\circ\text{C}$ under nitrogen for 2 h to form a brown transparent liquid. A total of 1 mL of this solution was taken and injected into the mercury chloride/oleylamine (HgCl_2 /OAm) solution, and was reacted at $115\text{ }^\circ\text{C}$ for 3–8 min. We removed the reaction solution out of the glove box and used cold water to end the reaction. After the end of the reaction, the HgSe CQDs solution was placed in a centrifuge tube. A total of 1 mL of 1-dodecyl mercaptan (DDT), 20 drops of didecyldimethylammonium bromide (DDAB), and 15 mL of methanol (MeOH) were added to the centrifuge tube. The solution in the centrifuge tube was centrifuged at 7500 r.p.m for 6 min. After centrifugation, the supernatant was decanted, and the remaining pellet was dissolved in chlorobenzene and filtered through a disposable filter.

The photocurrent spectrum of the material with Nicolet iS20 FTIR (Thermo Fisher Scientific, Waltham, MA, USA) was measured. The FTIR implemented 500,000:1 signal-to-noise ratio and 0.25 cm^{-1} spectral resolution.

Photoconductance spectra was measured with a standard Thermo Scientific Nicolet iS20 FTIR Spectrometer. The internal light was reflected in the sample with a gold mirror. The samples were biased with a 3 V battery in series. The current across the sample was sent to transimpedance amplifier Femto-200 with a gain of 10,000 before being sent back to the FTIR input.

3. Results and Discussion

3.1. Absorption Spectra

The Transmission Electron Microscope (TEM) image of HgSe CQDs with a synthesis temperature of $115\text{ }^\circ\text{C}$ and a synthesis time of 5 min is shown in Figure 1a. The average size of CQDs is 4.7 nm and the size distribution is uniform with the standard deviation of 0.5 nm (Supplementary Materials Figure S2). As can be seen in Figure 1b, the size of the CQDs can be varied by changing the synthesis temperature and time [21,22]. Changing the size of CQDs can achieve the movement of the absorption spectrum. The intraband absorption peak of HgSe CQDs is between $2000\text{--}3000\text{ cm}^{-1}$, and the absorption peak will be redshifted by increasing the reaction time. The relationship between CQDs of different sizes and energy bands is shown in Figure 1c. When the size of CQDs is "small", the Fermi level is lower than Se states, and the HgSe CQDs are defined as " n^- type". When the size of CQDs is "medium", the energy gaps become smaller, and the band shift. As a result, the Fermi level is in Se state, which we define as two electrons in conduction band per CQD [17]. When the size of CQDs is "large", the Fermi level is higher than Se states, and the HgSe CQDs are defined as " n^+ type". By changing the size of CQDs, the position of the absorption peaks in intraband and interband can be changed in Figure 1b. HgSe intraband photodetector can specifically detect signals in the Mid-IR range, possessing potential application in gas detection such as CO_2 with a signature absorption of 2400 cm^{-1} .

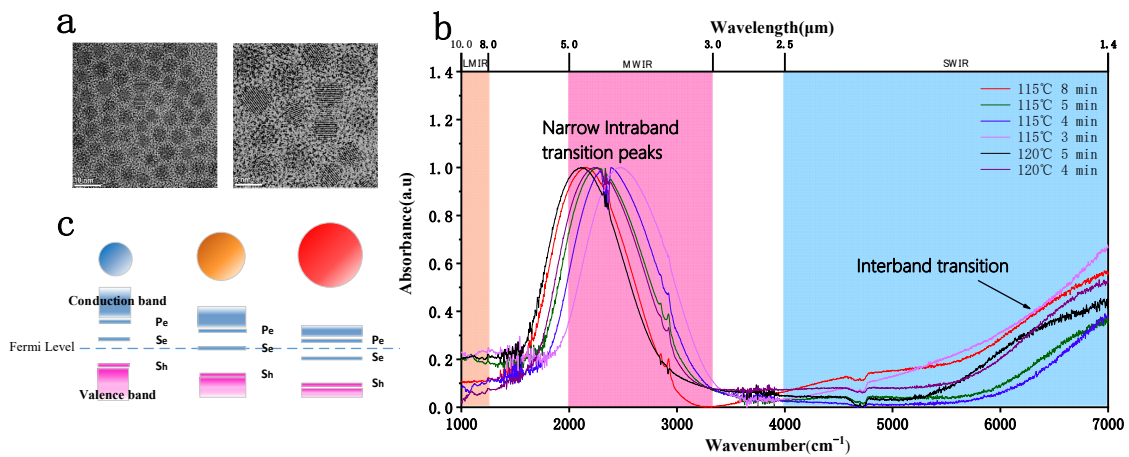


Figure 1. Characterization of HgSe CQDs materials. (a) TEM images of HgSe CQDs with a particle diameter of 4.7 nm and standard deviation of 0.5 nm. (b) Absorption spectra of HgSe CQDs. (c) Diagram of the relationship between the size of CQDs and energy bands.

3.2. Transport Properties of HgSe CQDs

Transport properties such as carrier type, carrier density, and carrier mobility greatly affect the photodetector performance. We can judge the performance of the material by measuring the carrier type and mobility of the HgSe film [23]. This information is given by the field effect transistor (FET) measurement. HgSe CQDs film is spin-coated on 300 nm SiO₂/Si substrate, which has a layer of interdigitated electrodes. A solid ligands exchange process with an ethanedithiol/hydrochloric acid (EDT/HCl) solution is followed. In this process, short ligands would displace the long chain OAm ligands between CQDs. After the ligand exchange, we rinse the film with isopropanol (IPA).

The HgSe/EDT CQD film is measured by a field effect transistor circuit. Whether CQDs are “n⁻ type” or “n⁺ type” can be determined by the slope sign of the FET transfer curves around zero gate potential. A schematic diagram of the FET structure is shown in Figure 2a.

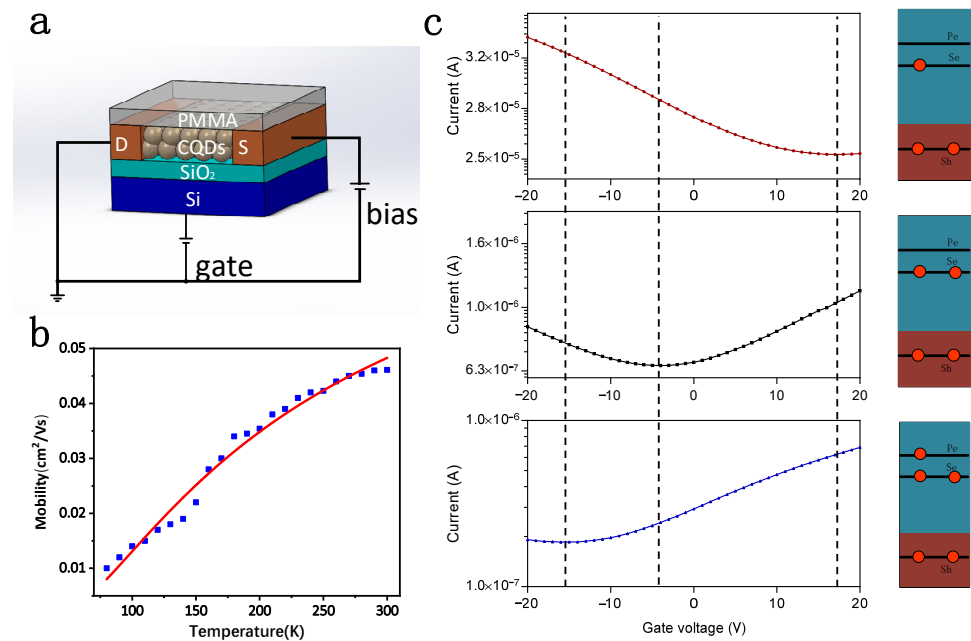


Figure 2. Transport study on HgSe CQDs. (a) Schematic diagram of the field effect pipe structure. (b) Carrier mobility at different temperatures and mobility fitted with Marcus theory as a function of temperature. (c) FET source-drain current as a function of voltage for HgSe/EDT at 80 K.

For QDs photodetectors, dark current and noise are important figures of merit. The shot noise has a great influence on the QDs photoconductivity detectors, and the formula for shot noise is shown in Equation (1):

$$i_n = \sqrt{4eI_{dark}} \quad (1)$$

where e is the electron charge, I_{dark} is the dark current of the photodetector.

The dark current is an important factor affecting the noise in Equation (1) and the root cause is the thermally excited electron-hole pairs. Therefore, the dark current has an exponential relationship with the temperature [24]. For photodetectors with intraband transition, the dark current was minimal at low temperature [25]. Therefore, after using liquid nitrogen to cool down to 80 K, the dark current is effectively reduced. The curve of FET source-drain current as a function of voltage for HgSe/EDT at 80 K is shown in Figure 2c.

In addition to cooling down to reduce the dark current, the effect of the dark current can also be reduced by adjusting the number of electrons filled in the 1Se band. By varying the temperature and time of synthesis, the number of electrons filled by HgSe QDs in the 1Se band can be regulated. In Figure 2c, when the number of doped electrons is two, the dark current is minimal. Compared with “n⁻ type” or “n⁺ type” QDs, the QDs with fully doped Se state have a ten-fold reduction in dark current.

The mobility of HgSe/EDT thin films can be calculated through the FET circuit, and the mobility calculation formula is as follows [26]:

$$\mu_{FET} = \frac{L}{WC_iV_D} \bullet \frac{\Delta I_D}{\Delta V_G} \quad (2)$$

Among them, the thickness of silica (SiO₂) is 300 nm, $C_i = 1.15 \times 10^{-4} \text{ F/m}^2$ is the capacitance, $L = 10 \mu\text{m}$ is the gap, $W = 1000 \mu\text{m} \times 50$ is total channel width, “50” is the number of channels, and $V_D = 1 \text{ V}$ is drain voltage. $\frac{\Delta I_D}{\Delta V_G}$ is the slope of the transfer current and the gate voltage. After calculation, the mobility of HgSe films exchanged with EDT can reach $0.046 \pm 0.002 \text{ cm}^2/\text{Vs}$ at room temperature.

Figure 2b shows the mobility curve with temperature. The low temperature limits the movement of the carrier, and the carrier mobility decreases to $0.012 \pm 0.001 \text{ cm}^2/\text{Vs}$ in Figure 2b. The increase in temperature will lead to less binding of the carrier and an upward trend in the mobility rate. After 260 K, the migration rate’s growth rate slows down. The highest mobility is $0.046 \pm 0.002 \text{ cm}^2/\text{Vs}$ at room temperature. The trend of migration change can be explained by Marcus theory:

$$\mu_{FET} = Con \exp(-(\gamma + \Delta G)^2 / 4\gamma k_B T) \quad (3)$$

where Con is the constant, ΔG the energy difference caused by uneven size of QDs, $k_B = 1.380649 \times 10^{-23} \frac{\text{J}}{\text{K}}$ is the Boltzmann constant. The polarization effect of the medium around the carrier is given by the recombinant energy γ [27]. γ is expressed by the following equation:

$$\gamma = \frac{e}{4\pi\epsilon_0} \left(\frac{1}{a} - \frac{1}{2(a+b)} \right) \left(\frac{1}{\epsilon_1} - \frac{1}{\epsilon_{st}} \right) \quad (4)$$

where $e = 1.6 \times 10^{-19} \text{ C}$ is the elementary charge, $\epsilon_0 = 8.85 \times 10^{-12} \frac{\text{F}}{\text{m}}$ is the vacuum permittivity, $a = 2.3 \text{ nm}$ is the radius of the QDs, $b = 1 \text{ nm}$ is the spacing between QDs, $\epsilon_1 = 6.8$ is the optical dielectric constant of matrix surrounding QDs which is measured by the ellipsometry, $\epsilon_{st} = 10.9$ is the static dielectric constant. We can get $\gamma = 16 \text{ meV}$, $G = 16.9 \text{ meV}$ and $Con = 0.09$ by the Marcus fitting calculation. The disorder energy is similar to the values in the previous reference [26].

3.3. Photocurrent

The photocurrent and dark current curves of the HgSe CQDs intraband photodetector are shown in Figure 3a. As shown in Figure 3a, the $\frac{I_{\text{photocurrent}}}{I_{\text{darkcurrent}}} = 10\%$ when the bias voltage is ± 3 V. Compared with previous studies [28], our work effectively improves the light–dark current ratio of pure HgSe quantum dots thin films. Figure 3b shows the photocurrent spectrum of the HgSe detector at 80 K. The photocurrent spectrum of the HgSe intraband photodetector is narrow at 80 K and the photoconduction is from 2000–3000 cm^{-1} in Figure 3b. The HgSe photodetector has a narrow photoresponse, making it possible to react more sensitively to change in the outside world. And the HgSe intraband transition photodetector has an obvious photocurrent at low temperatures, so it can be widely used in harsh low temperature environments for detection.

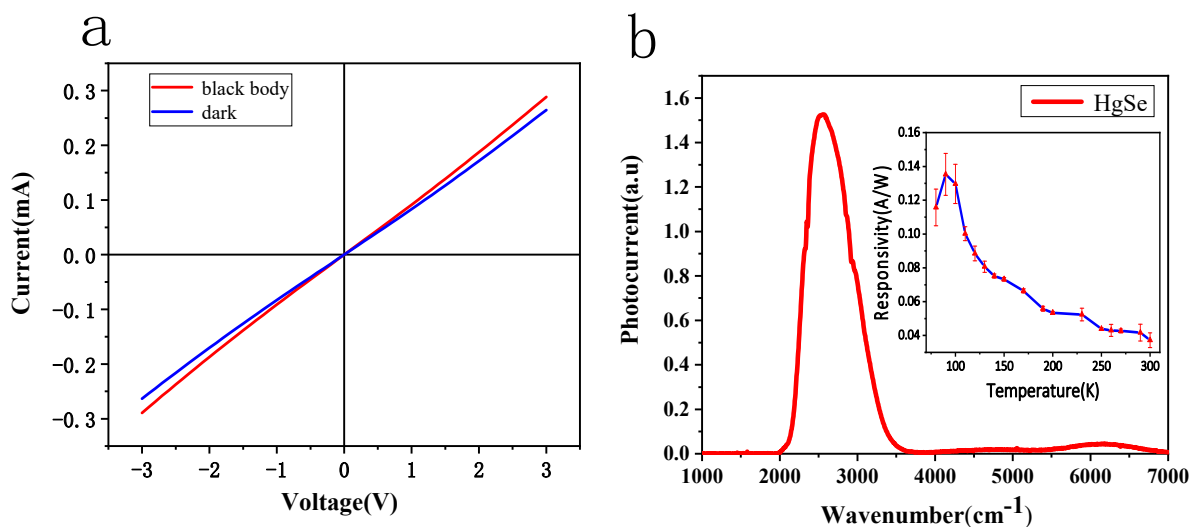


Figure 3. Photocurrent on HgSe CQDs. (a) HgSe CQDs as a function of current and voltage at 80 K. The red line represents the photocurrent when photodetector is illuminated by blackbody, and the blue line represents the dark current. (b) Photocurrent spectra with HgSe CQDs films at 80 K. The right inset graph shows the responsivity of HgSe CQDs thin films as a function of temperature.

The responsivity is calculated by measuring the photocurrent of the HgSe photoconductor device. The right-inset graph in Figure 3b shows the responsivity of HgSe thin films as a function of temperature (Supplementary Materials). It can be seen from the figure that the responsivity reaches a maximum of 0.135 ± 0.012 A/W at 90 K. It gradually heats up after 90 K, and the responsivity gradually decreases.

HgSe CQDs intraband photodetectors have narrow band spectral response in 2000–3000 cm^{-1} , which can be used in gas detection. Due to the detection capability of the intraband photodetectors in the infrared field, it can be applied to the fields of infrared imaging, target recognition, and radar detection, and other fields. Through the study of HgSe CQDs intraband photodetectors, we found that HgSe CQDs intraband photodetectors have better photoelectric performance at low temperatures. Therefore, HgSe CQDs intraband photodetectors can be applied to infrared detection in a low temperature environment. HgSe CQDs intraband photodetectors have broad application prospects.

4. Conclusions

In summary, this paper mainly introduces the intraband photodetector based on HgSe CQDs. Its intraband absorption spectrum is between 2000–3000 cm^{-1} . We provide a method to achieve accurate electron doping through repeated experiments to suppress the dark currents. When the fully doped Se state is obtained experimentally, the effect of the dark current is minimal. Compared with “ n^- type” and “ n^+ type” CQDs, our dark current is effectively reduced by a factor of 10 measured by the field effect transistor. The mobility

of HgSe/EDT films measured by FET can reach $0.046 \pm 0.002 \text{ cm}^2/\text{Vs}$. We experimentally calculate the responsivity of HgSe QDs to be $0.135 \pm 0.012 \text{ A/W}$. Through the study of the performance of the intraband infrared photodetector, the selection of infrared photodetector materials can be broadened, which is of great significance for infrared detection.

Supplementary Materials: The following are available online at <https://www.mdpi.com/article/10.3390/coatings12040467/s1> [29,30]. Figure S1. Bands diagram; Figure S2. TEM image and size analysis of the 5 mins sample.

Author Contributions: Conceptualization, X.Z., X.T. and M.C.; Formal analysis, X.Z. and X.T.; Funding acquisition, M.C.; Investigation, G.M.; Methodology, X.Z.; Project administration, M.C.; Supervision, X.T. and M.C.; Validation, M.C.; Visualization, X.T.; Writing—original draft, X.Z.; Writing—review & editing, X.Z., G.M., X.T. and M.C. All authors have read and agreed to the published version of the manuscript.

Funding: This work is funded by NSFC 62105022, Beijing Nova Program Z211100002121069.

Institutional Review Board Statement: Not applicable.

Informed Consent Statement: Not applicable.

Data Availability Statement: Not applicable.

Conflicts of Interest: The authors declare no conflict of interest.

References

1. Lhuillier, E.; Guyot-Sionnest, P. Recent Progresses in Mid Infrared Nanocrystal based Optoelectronics. *IEEE J. Sel. Top. Quantum Electron.* **2017**, *23*, 6000208. [CrossRef]
2. Livache, C.; Goubet, N.; Gréboval, C.; Martinez, B.; Ramade, J.; Qu, J.; Triboulin, A.; Cruguel, H.; Baptiste, B.; Klotz, S.; et al. Effect of Pressure on Interband and Intraband Transition of Mercury Chalcogenide Quantum Dots. *J. Phys. Chem. C* **2019**, *123*, 13122–13130. [CrossRef]
3. Phillips, J. Evaluation of the fundamental properties of quantum dot infrared detectors. *J. Appl. Phys.* **2002**, *91*, 4590–4594. [CrossRef]
4. Kershaw, S.V.; Susha, A.S.; Rogach, A.L. Narrow bandgap colloidal metal chalcogenide quantum dots: Synthetic methods, heterostructures, assemblies, electronic and infrared optical properties. *Chem. Soc. Rev.* **2013**, *42*, 3033–3087. [CrossRef]
5. Malinowski, P.E.; Georgitzikis, E.; Maes, J.; Vamvaka, I.; Frazzica, F.; Van Olmen, J.; De Moor, P.; Heremans, P.; Hens, Z.; Cheyns, D. Thin-Film Quantum Dot Photodiode for Monolithic Infrared Image Sensors. *Sensors* **2017**, *17*, 2867. [CrossRef]
6. Martyniuk, P.; Rogalski, A. Quantum-dot infrared photodetectors: Status and outlook. *Prog. Quantum Electron.* **2008**, *32*, 89–120. [CrossRef]
7. Keuleyan, S.; Lhuillier, E.; Guyot-Sionnest, P. Synthesis of Colloidal HgTe Quantum Dots for Narrow Mid-IR Emission and Detection. *J. Am. Chem. Soc.* **2011**, *133*, 16422–16424. [CrossRef] [PubMed]
8. Keuleyan, S.; Lhuillier, E.; Brajuskovic, V.; Guyot-Sionnest, P. Mid-infrared HgTe colloidal quantum dot photodetectors. *Nat. Photonics* **2011**, *5*, 489–493. [CrossRef]
9. Guyot-Sionnest, P.; Roberts, J.A. Background limited mid-infrared photodetection with photovoltaic HgTe colloidal quantum dots. *Appl. Phys. Lett.* **2015**, *107*, 253104. [CrossRef]
10. Deng, Z.; Jeong, K.S.; Guyot-Sionnest, P. Colloidal Quantum Dots Intraband Photodetectors. *ACS Nano* **2014**, *8*, 11707–11714. [CrossRef] [PubMed]
11. Livache, C.; Martinez, B.; Goubet, N.; Greboval, C.; Qu, J.; Chu, A.; Royer, S.; Ithurria, S.; Silly, M.G.; Dubertret, B.; et al. A colloidal quantum dot infrared photodetector and its use for intraband detection. *Nat. Commun.* **2019**, *10*, 2125. [CrossRef]
12. Ramiro, I.; Ozdemir, O.; Christodoulou, S.; Gupta, S.; Dalmasas, M.; Torre, I.; Konstantatos, G. Mid- and Long-Wave Infrared Optoelectronics via Intraband Transitions in PbS Colloidal Quantum Dots. *Nano Lett.* **2020**, *20*, 1003–1008. [CrossRef]
13. Li, S.; Xia, J. Intraband optical absorption in semiconductor coupled quantum dots. *Phys. Rev. B Condens. Matter* **1997**, *55*, 15434–15437. [CrossRef]
14. Sato, S.A.; Lucchini, M.; Volkov, M.; Schlaepfer, F.; Gallmann, L.; Keller, U.; Rubio, A. Role of intraband transitions in photocarrier generation. *Phys. Rev. B* **2018**, *98*, 035202. [CrossRef]
15. Qu, J.; Goubet, N.; Livache, C.; Martinez, B.; Amelot, D.; Gréboval, C.; Chu, A.; Ramade, J.; Cruguel, H.; Ithurria, S.; et al. Intraband Mid-Infrared Transitions in Ag₂Se Nanocrystals: Potential and Limitations for Hg-Free Low-Cost Photodetection. *J. Phys. Chem. C* **2018**, *122*, 18161–18167. [CrossRef]
16. Park, M.; Choi, D.; Choi, Y.; Shin, H.B.; Jeong, K.S. Mid-Infrared Intraband Transition of Metal Excess Colloidal Ag₂Se Nanocrystals. *ACS Photonics* **2018**, *5*, 1907–1911. [CrossRef]

17. Melnychuk, C.; Guyot-Sionnest, P. Auger Suppression in n-Type HgSe Colloidal Quantum Dots. *ACS Nano* **2019**, *13*, 10512–10519. [[CrossRef](#)]
18. Chen, M.; Guyot-Sionnest, P. Reversible Electrochemistry of Mercury Chalcogenide Colloidal Quantum Dot Films. *ACS Nano* **2017**, *11*, 4165–4173. [[CrossRef](#)]
19. Martinez, B.; Livache, C.; Notemngnou Mouafo, L.D.; Goubet, N.; Keuleyan, S.; Cruguel, H.; Ithurria, S.; Aubin, H.; Ouerghi, A.; Doudin, B.; et al. HgSe Self-Doped Nanocrystals as a Platform to Investigate the Effects of Vanishing Confinement. *ACS Appl. Mater. Interfaces* **2017**, *9*, 36173–36180. [[CrossRef](#)]
20. Chen, M.; Shen, G.; Guyot-Sionnest, P. Size Distribution Effects on Mobility and Intraband Gap of HgSe Quantum Dots. *J. Phys. Chem. C* **2020**, *124*, 16216–16221. [[CrossRef](#)]
21. Grigel, V.; Sagar, L.K.; De Nolf, K.; Zhao, Q.; Vantomme, A.; De Roo, J.; Infante, I.; Hens, Z. The Surface Chemistry of Colloidal HgSe Nanocrystals, toward Stoichiometric Quantum Dots by Design. *Chem. Mater.* **2018**, *30*, 7637–7647. [[CrossRef](#)]
22. Martinez, B.; Livache, C.; Meriggio, E.; Xu, X.Z.; Cruguel, H.; Lacaze, E.; Proust, A.; Ithurria, S.; Silly, M.G.; Cabailh, G.; et al. Polyoxometalate as Control Agent for the Doping in HgSe Self-Doped Nanocrystals. *J. Phys. Chem. C* **2018**, *122*, 26680–26685. [[CrossRef](#)]
23. Lan, X.; Chen, M.; Hudson, M.H.; Kamysbayev, V.; Wang, Y.; Guyot-Sionnest, P.; Talapin, D.V. Quantum dot solids showing state-resolved band-like transport. *Nat. Mater.* **2020**, *19*, 323–329. [[CrossRef](#)]
24. Mahmoodi, A.; Dehdashti Jahromi, H.; Sheikhi, M.H. Dark Current Modeling and Noise Analysis in Quantum Dot Infrared Photodetectors. *IEEE Sens. J.* **2015**, *15*, 5504–5509. [[CrossRef](#)]
25. Liu, H.; Zhang, J.; Ackerman, M.M. Dark current and noise analyses of quantum dot infrared photodetectors. *Appl. Opt.* **2012**, *51*, 2767–2771. [[CrossRef](#)] [[PubMed](#)]
26. Chen, M.; Shen, G.; Guyot-Sionnest, P. State-Resolved Mobility of $1 \text{ cm}^2/(\text{Vs})$ with HgSe Quantum Dot Films. *J. Phys. Chem. Lett.* **2020**, *11*, 2303–2307. [[CrossRef](#)]
27. Prodanovic, N.; Vukmirovic, N.; Ikonc, Z.; Harrison, P.; Indjin, D. Importance of Polaronic Effects for Charge Transport in CdSe Quantum Dot Solids. *J. Phys. Chem. Lett.* **2014**, *5*, 1335–1340. [[CrossRef](#)]
28. Izquierdo, E.; Dufour, M.; Chu, A.; Livache, C.; Martinez, B.; Amelot, D.; Patriarche, G.; Lequeux, N.; Lhuillier, E.; Ithurria, S. Coupled HgSe Colloidal Quantum Wells through a Tunable Barrier: A Strategy to Uncouple Optical and Transport Band Gap. *Chem. Mater.* **2018**, *30*, 4065–4072. [[CrossRef](#)]
29. Chen, M.; Lan, X.; Tang, X.; Wang, Y.; Hudson, M.H.; Talapin, D.V.; Guyot-Sionnest, P. High Carrier Mobility in HgTe Quantum Dot Solids Improves Mid-IR Photodetectors. *ACS Photonics* **2019**, *6*, 2358–2365. [[CrossRef](#)]
30. Tang, X.; Ackerman, M.M.; Guyot-Sionnest, P. Thermal imaging with plasmon resonance enhanced HgTe colloidal quantum dot photovoltaic devices. *ACS Nano* **2018**, *12*, 7362–7370. [[CrossRef](#)] [[PubMed](#)]